Integration of a parabolic-trough solar field with solid-solid latent storage in an industrial process with different temperature levels

Mario Biencinto [a],[*], Rocío Bayón [a], Lourdes González [a], Rosa Christodoulaki [b], Esther Rojas [a]

[a] Plataforma Solar de Almería (PSA-CIEMAT), Av. Complutense 40, 28040 Madrid, Spain
[b] Centre for Renewable Energy Sources and Saving, Solar Thermal Systems Department, Marathonos av. 19 klm, 19009 Pikermi Hellas, Greece

ARTICLE INFO

ABSTRACT

The aim of this work is to analyse the integration of solar industrial process heat with novel latent heat storage systems by means of a representative case study that has a demand profile with different temperature levels. To that end, an innovative thermal storage system is proposed to support the contribution of the solar field to the industrial heat demand. The storage system considered is based on the latent heat of the solid–solid transition of pentaglycerine and it seems particularly interesting for industrial applications with space limitations and low temperature differences. Additionally, it may suppose further advantages in terms of corrosion, degradation and low cost of raw material. Thermal tests have confirmed the suitability of pentaglycerine as storage material for such applications. In this case study, a solar field with parabolic-trough collectors coupled to a pasteurization process has been considered. To analyse the expected behaviour of the proposed system, a simulation model has been developed in TRNSYS. This model defines, for the first time in the literature, a complete set of operation modes and control strategies specific to concentrating solar collectors for industrial process heat applications with latent storage, able to deal with the required variable temperature levels. Annual simulations have been performed using locations and meteorological data of Graz (Austria) and Plataforma Solar de Almería (Spain). The simulation results show that the percentage of annual heat demand covered with solar energy could be increased from 20% to 27% in Graz or from 40% to 52% in the PSA by using 3 h of latent heat storage.

1. Introduction

According to the International Energy Agency [1], the amount of thermal energy required worldwide by industry was 86 EJ in 2017, which represents about 73% of the total industrial energy consumption. Since approximately 52% of that heat demand lies in temperatures below 400 °C [2], it can be provided by concentrating solar technologies such as parabolic-trough collectors. Several industrial sectors can be identified as intensive heat consumers within these temperature ranges. These industries include chemical synthesis, food and beverage, textile, wood processing, pulp and paper, mining and machinery; with thermal processes like evaporation, distillation, pasteurization, cleaning, washing and drying.

Solar Heat for Industrial Processes (SHIP) is an emerging field of business development with high potential among solar heating and cooling applications [3]. Extensive analyses of SHIP potential, solar technologies and simulation tools can be found in the review works by

Kumar et al. [4] and Sharma et al. [5]. In addition, the SHIP potential in specific areas and sectors has been assessed. For instance, the integration of SHIP systems into dairy industries in India may lead to average solar fractions from 18 to 32% [6]. From these studies, it can be concluded that solar technologies implemented in industrial processes working at low and medium temperatures are ready for the market and offered by industry. According to the AEE INTEC SHIP database [7] and a SHIP supplier survey carried out by the consulting company SOLRICO [8], at least 741 SHIP plants with an overall collector area of 662,648 m^2 (567 MW_{th}) were installed worldwide by the end of 2018 [9]. However, the development of SHIP applications still faces some challenges that result in a modest share of about 0.3% of total installed solar thermal capacity [3].

The complex interaction of various energy supply technologies (mainly solar energy and fossil sources) for industrial sites requires new integration designs that ensure energy flows to be used, stored and combined in an optimized way. New storage concepts play a crucial role in such innovative designs. In this way, both sensible [10] and latent

* Corresponding author.

E-mail addresses: mario.biencinto@ciemat.es (M. Biencinto), rocio.bayon@ciemat.es (R. Bayón), lourdes.gonzalez@ciemat.es (L. González), christodoulaki@cres.gr (R. Christodoulaki), esther.rojas@ciemat.es (E. Rojas).

Nomenclature

A	area, m^2
c_p	specific heat capacity at constant pressure, J·kg^{-1}·K^{-1}
G_b	direct normal solar irradiance, W/m^2
$K(\theta)$	incidence angle modifier, -
m	mass, kg
$\dot{m}$	mass flow rate, kg/s
Q	thermal energy, J
$\dot{Q}$	thermal power, W
t	time, s
T	temperature, °C
U	heat transfer coefficient, W·m^{-2}·K^{-1}
x	storage level, -

Acronyms

CSP	concentrating solar power
DNI	direct normal solar irradiance (equivalent to G_b)
HTF	heat transfer fluid
HX	heat exchanger
IP	industrial process
LHS	latent heat storage
PG	pentaglycerine
PSA	Plataforma Solar de Almería
PTC	parabolic-trough collector

PCM	phase change material
RMSE	root mean squared error
SF	solar field
SHIP	solar heat for industrial processes
SS	solid–solid
TES	thermal energy storage

Greek symbols

Δ	increment or variation
η	efficiency or performance factor, -
θ	incidence angle, °

Subscripts

amb	ambient
c	net solar collection
clean	cleanliness
in	inlet
loss	thermal losses
min	minimum
opt,0°	peak optical
out	outlet
ref	reference or set-point value
sh	shadowing
transf	transferred
u	useful

[11] heat storage solutions have been proposed for SHIP applications. The integration of storage technologies for techno-economically optimized SHIP concepts will require a proper modelling and simulation of their expected behaviour within the simulation software, enabling the matching of variable heat sources and variable load profiles.

The integration of industrial processes, solar collectors and thermal energy storage (TES) systems has been widely addressed and simulated in various research studies. For instance, the work of Baniassadi et al. [12] proposed a method for the optimum integration of generic TES systems in low-temperature SHIP, resulting in solar fractions from 17 to 47%. Commonly, sensible TES based on hot water tanks is considered for SHIP systems. A case study of a specific SHIP application for a dairy process with evacuated collectors and water tanks was analysed in the work by Maillot et al. [13], including the simulation of different integration schemes between the solar heat and the TES system. Another example of SHIP analysis with evacuated collectors and a hot water tank as TES, using gas boiler backup, can be found in [14]. In the case of concentrating solar collectors, two works are worth mentioning: a case study of SHIP integration in a pasta factory [15], choosing parabolic-trough collectors (PTCs) among several concentrating solar technologies, that resulted in a solar fraction of 23%; and a co-simulation model [16] of a SHIP application with PTCs and TES, using the software tools Modelica and TRNSYS, which yielded 67% solar fraction for locations in Southern Europe. Nevertheless, the integration of such systems in processes that involve different temperature levels may represent a challenge for the system design. In this way, the work of Allouhi et al. [17] proposed an optimization procedure for a SHIP application with different temperature levels in a milk processing factory in Morocco. The system included evacuated-tube collectors and a water tank as TES, obtaining an overall annual solar fraction of 41%.

The use of storage concepts based on latent heat can be particularly interesting for SHIP applications with low temperature differences, even when daily demand profile includes various temperature levels. Since latent heat storage (LHS) occurs at constant temperature, exergy losses are low. In addition, charge and discharge processes can be scheduled whenever they are more convenient to optimize the heat flows involved between the solar field and the industrial process. To that end, operation

strategies depending on system variables such as process demand, solar radiation and state of charge, should be defined to improve the overall system performance. In order to analyse and optimize SHIP concepts with such storage systems, the development of simulation models that accurately reproduce the behaviour of the whole circuit can be very helpful.

In LHS systems, phase change materials (PCMs) are used as storage media. Among them, PCMs based on solid–solid transitions (SS-PCMs) are of great practical interest because they present several advantages such as lack of leakages, no volume change during phase transition together with low material degradation and container corrosion risk since liquid state is not attained [18]. For the case of SHIP applications with working temperatures below 100 °C, organic materials based on polyalcohols like pentaerythritol, pentaglycerine, neopentylglycol and mixtures thereof could be appropriate SS-PCMs [18]. Depending on the polyalcohol mixture composition, SS transition temperatures between 40 °C and 188 °C can be found [19]. The energy density of these mixtures is usually higher than that of storage media based on sensible heat at similar temperatures, such as water. Since space availability is commonly a key issue for SHIP applications, LHS systems with polyalcohols may thus represent an attractive solution to land restrictions in industrial areas. Furthermore, these polyalcohols can be either combined with other compounds to form composites or encapsulated by the provider. Since the thermal conductivity of these materials is commonly low, both solutions can be useful to improve the heat transfer between the working fluid and the SS-PCM. In this way, some experimental studies [20,21,22] have been conducted to investigate these options for thermal energy storage, but they focused on the SS-PCM synthesis and the analysis of their thermal properties rather than their integration into real LHS devices suitable for SHIP applications.

Several studies address the integration of solar thermal technologies with latent storage. A review of numerical studies on solar collectors integrated with LHS systems employing fins or nanoparticles was carried out by Bazri et al. [23]. Also, an analytical study of charging/discharging processes in LHS for solar water heaters was conducted by the same authors [24], comparing different PCMs based on paraffin wax. In addition, the work of Pagkalos et al. [25] evaluated numerically the use

of paraffin PCM as storage media. A specific case of LHS in a SHIP application of solar dryer in the wood sector was simulated by Lamrani and Draoui [26]. However, these works only consider PCMs based on solid–liquid transitions and they do not address operation strategies of the whole SHIP system or demand profiles with different temperature levels. On the other hand, the article of Zhao et al. [27] proposed simulation models and operation modes for solar heating systems and latent storage, but it was focused on flat-plate collectors for building heating, which present a much simpler operation and demand profile than industrial process heat applications with concentrating solar collectors.

In summary, no studies have been found in the literature that address the integration of SHIP applications with concentrating solar collectors and LHS systems based on SS-PCMs, considering the interaction between the solar field, the storage system and a heat demand that involves different temperature levels. Moreover, the specific behaviour of such SHIP systems in terms of operation modes and strategies has not yet been studied. In this way, the aim of this article is to analyse the integration of SHIP concepts with LHS systems by means of a representative case study, establishing a suitable collection of operation modes able to deal with the different conditions that may occur. Also, this study intends to provide a preliminary figure of the expected differences in annual energy between systems with and without LHS for various locations. To this end, a one-dimensional quasi-dynamic model of parabolic-trough collectors, insulated pipes and latent storage has been developed in TRNSYS. This model combines both physical and empirical approaches and takes into account the different operating scenarios that may arise in such SHIP applications.

The case study analysed in this work is an industrial pasteurization process involving different temperature levels. To evaluate the behaviour and performance of the new SHIP concept, a parabolic-trough solar field with a LHS system using pentaglycerine as SS-PCM material is integrated into this industrial process. In addition, laboratory experimental tests have been performed to ensure the suitability of pentaglycerine as the latent storage medium. The described model is applied to simulate the whole system considering actual demand profiles and provide overall energy outputs for given periods. From the analysis of this case study, this article proposes a set of specific operating strategies broadly applicable to energy systems based on concentrating solar collectors and thermal storage systems.

2. System description

The system under investigation includes the industrial application defined by its demand profile, a parabolic-trough solar field (SF) with a certain number of solar thermal collectors and a storage system based on latent heat. The subsections below describe the main features of the industrial process (IP), the solar collector selected and the LHS system, together with the overall layout adopted.

2.1. Industrial process (IP)

The IP considered in this study is the pasteurization process of a dairy factory located in Graz, Austria. The heat supply to such process involves three different temperature levels with a specific daily profile of thermal power, provided by AEE-INTEC [28], which is the same for the whole year. This profile has a time step of 10 min and is represented in Fig. 1.

The heat demand of the IP starts every day at 10:30 at 85 °C. The required temperature is reduced to 74 °C at 12:00 and to 40 °C at 14:30. Temperature is increased again to 74 °C at 15:30 and maintained at this level until the end of daily operation at 19:00. A fixed temperature difference of 7 °C between inlet and outlet is observed at each temperature level. Besides, the mass flow rate of the process fluid is the same, 11.11 kg/s, during the whole daily operation period, resulting in a constant heat requirement around 293 kW$_{th}$.

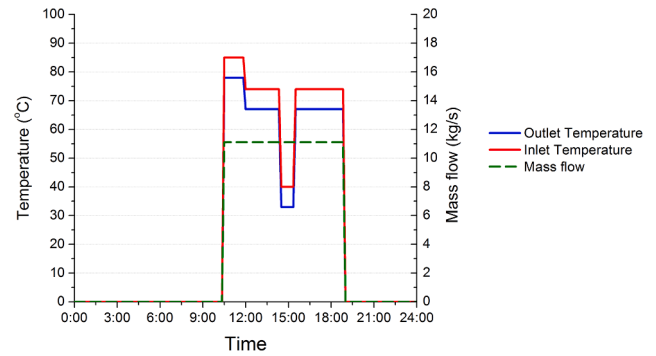A solar thermal system using pressurized water as heat transfer fluid

Fig. 1. Daily evolution of inlet and outlet temperatures and mass flow rate of milk in the pasteurization process considered (source: AEE-INTEC [28]).

(HTF) is going to be coupled to the described process, considering integration on process level. Since different working fluids are going to be used in the SF (pressurized water) and the IP (milk), a heat exchanger (HX) is required between both fluids. The HX thus represents the integration point between the solar thermal system and the IP.

The daily demand profile of Fig. 1 spans from 10:30 to 19:00. This time frame does not fit with available solar energy on most days of the year. In this way, the inclusion of a TES system may be advantageous to match the IP energy demand with the available solar resource.

2.2. Parabolic-trough collector (PTC)

Even though non-concentrating collectors can also be considered, the conditions established by the IP in terms of temperature and mass flow rate are compatible with the use of solar collectors with medium concentration ratio, such as parabolic troughs. Parabolic-trough collectors are line-focus collectors that concentrate the direct solar irradiance by means of a cylindrical reflective surface of parabolic section and track the sun by rotation around an axis. The reflected energy is concentrated onto a receiver tube located at the focal line of the parabola, thus heating the heat transfer medium that circulates inside the tube. The solar concentration and sun tracking system of PTCs make them more efficient per unit collection area than non-concentrating technologies, such as flat-plate collectors or evacuated tubes, and hence an advisable choice for industrial applications with limited available space.

Considering the temperature level demanded by the IP, a small parabolic-trough collector with sun tracking system, NEP SOLAR Poly-Trough 1800, is chosen for this application. The main parameters of the base module of a standard PolyTrough 1800 collector are shown in Table 1 [29].

Table 1
Parameters of the base module of a PolyTrough 1800 collector.

Parameter	Value
Focal length (mm)	647
Aperture width (mm)	1845
Collector Length (m)	10
Absorber tube diameter (mm)	34
Absorber tube wall thickness (mm)	1.5
Glass tube diameter (mm)	56
Glass tube wall thickness (mm)	2.5
Concentration ratio	17.3
Acceptance angle (°)	1
Gross area (m^2)	21.782
Rim angle (°)	71
Max. incident angle (°)	86.4
Net aperture area (m^2)	18.45
Absorber area (m^2)	1.079
Weight of complete module (kg)	700

2.3. Thermal energy storage (TES) system

As said above, the combination of a TES system with the PTC solar field would allow supplying energy to the IP when solar resource is not available. Taking into account that the temperature values required by the IP are lower than 100 °C and that the HTF chosen for the SF is pressurized water, a sensible heat storage system based on a simple water tank might also be suitable for this application. However, using a LHS material should strongly reduce the volume required for the storage system, which is particularly attractive for industrial processes with space limitations and/or water restrictions [25]. Moreover, in the case of a LHS system, heat is released at constant temperature. This also represents an advantage in terms of exergy losses if we compare with a water storage module which requires a higher temperature gradient for exchanging sensible heat.

The TES system implemented in this SHIP application uses the latent heat of a SS-PCM. Taking into account the temperature ranges of the IP considered (see Section 2.1) and the preliminary feasibility tests previously performed with various SS-PCMs [30], pure pentaglycerine (PG) seems to be the most suitable one. Moreover, as reported by former studies [31], it is not expensive with a price around 1.5 €/kg specific cost of raw material. The thermophysical properties of pentaglycerine relevant for this application, and taken from the literature [19,31,32], are summarized in Table 2.

According to our preliminary assessment tests consisting in heating/cooling cycles carried out in an oven, pentaglycerine undergoes SS transition in the range of [84.4, 85.4] °C upon heating and in the range [79.5, 83.0] °C upon cooling [30].

On the other hand, if we take into account the properties shown in Table 2, the volume of raw material needed for pentaglycerine would be around 10 times lower than for water, thus representing a significant reduction in the space required by the storage system.

2.4. Solar field (SF) layout

The SF layout has been designed with the help of the dimensioning tool [33] developed within the INSHIP project. Nominal power is determined from the demand profile of the IP depicted in Fig. 1 and reverse return is considered for the arrangement of distribution pipes. As a result, a solar field with 8 loops, each loop including 4 PolyTrough-1800 PTC modules has been defined for this application.

The overall layout for the whole system including TES, HX and the conventional process heat network is shown in the diagram of Fig. 2. The SF heats up the working fluid, which can be sent to the storage system or delivered to the IP via three-way valves. The HTF at the required temperature, obtained either from the SF or the storage system, is used to supply the heat demanded by the IP by means of a HX.

The bypass circuit (in dashed blue lines), parallel to the TES system circuit in Fig. 2, may be used either to enable the stand-alone operation of the SF for preheating purposes or to cool down the fluid obtained from the storage system in a discharge process, in order to provide the required inlet temperature to the IP.

Fig. 2 also includes the required dimensions for the SF: 42×44 m^2, considering 6 m of distance between collectors' rows, 2 m of extra length

Table 2
Thermophysical properties of pure pentaglycerine (PG) [19,31,32].

Parameter	Value
Molecular formula	$C_5H_{12}O_3$
Molecular weight (g/mol)	120.15
Density (kg/m^3)	1220
Thermal conductivity (W/m-K)	0.232
Specific heat capacity (kJ/kg.K)	2.8
SS transition temperature (°C)	81–82
SS transition latent heat (kJ/kg)	166–197
SS transition entropy (J/mol.K)	65.31

for piping on each row and a typical configuration with reverse return, which provides a suitable balance in pressure drop between rows for such a field size. In addition, the required area for this SF layout is considered small enough to fit with the usual land availability constraints of industrial areas.

3. Modelling approach

The simulation model described in this work has been developed in the TRNSYS software environment [34]. Some components have been taken from the TRNSYS standard library (from now on, referred as standard types) and some new components have been developed in-house. A screenshot of the TRNSYS model for the whole proposed system, including the SF, the storage system and the HX, is displayed in Fig. 3.

The TRNSYS model shown in Fig. 3 includes the SF control, collectors' loops, distribution pipes, the storage system, the HX, weather data and process data readers (standard Type9a), a radiation processor (standard Type16g) to calculate solar angles and a component (type293) to store variables for the next time step. In addition, equation editors are employed to adapt the corresponding variables to the model requirements and to obtain overall results, along with integrators (standard Type24) to sum up cumulative results (either daily or monthly values).

Both weather data and demand profile of the IP are supplied to the model as separate input files, so that a flexible simulation is allowed even with different time steps for each data (and, in turn, different from the simulation time step). Weather data include, for each time step considered, DNI and ambient temperature (T_{amb}) at the specific location, whereas process input data provide inlet and outlet temperatures, together with the mass flow rate of the process fluid, required by the IP.

The HX is simulated with the help of a standard component, Type5b, which models a zero capacitance sensible heat exchanger in counter-flow configuration. Given the hot and cold side inlet temperatures and flow rates, and including the specific heat capacity of source and load side fluids as parameters (c_p values of 4.19 kJ/kg.K for water and 3.77 kJ/kg.K for milk are applied), effectiveness is calculated for a given fixed value of the overall heat transfer coefficient. Based on typical heat transfer coefficients for plate heat exchangers in similar applications [35,36], the UA parameter (overall heat transfer coefficient times heat transfer area) considered in the simulation model is 54 kW/K (assuming $U = 900$ W/m^2.K and $A = 60$ m^2).

3.1. Meteorological data

The location of the dairy factory in which the selected IP takes place is Graz, Austria (47.071° N, 15.438° E), and the meteorological data to be used in annual yield simulations are taken from Meteonorm [37]. The time step of input data is 1 h for Graz and 5 min for the PSA.

Since the overall values of annual DNI for the considered location are significantly low (around 1150 kWh/m^2 as seen in Table 3), typical meteorological data from Plataforma Solar de Almería [38], Spain (37.097° N, 2.359° W), with an annual DNI value of 2071 kWh/m^2, will be used as reference to compare the results obtained for Graz. Calculated from hourly values, monthly values of DNI and average value of ambient temperature (T_{amb}) are summarized in Table 3 for either Graz or PSA locations.

3.2. Solar field model

The SF model simulates the thermal and hydraulic behaviour of PTC loops, distribution pipes, flow controllers and the rest of SF components. Basically, a steady-state approach that combines both physical and empirical expressions is followed to determine the thermal power yielded by the solar field in nominal conditions. Nevertheless, during non-stationary conditions, such as transient clouds, startup and shutdown
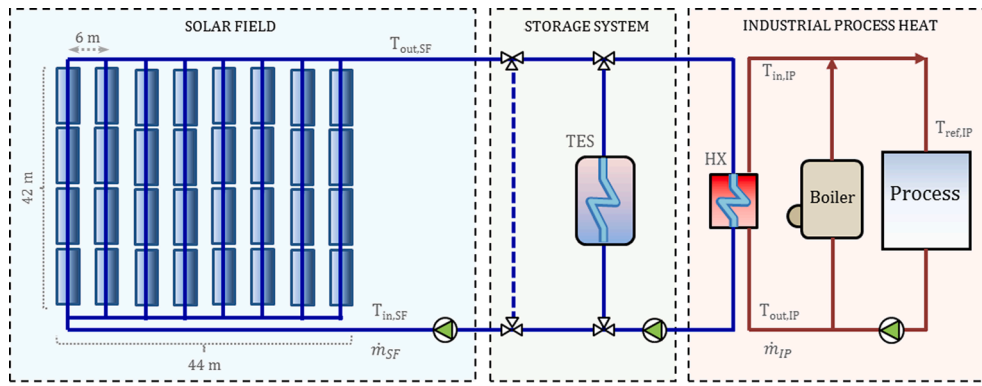
Fig. 2. Overall layout, main elements and solar field dimensions for the proposed system.
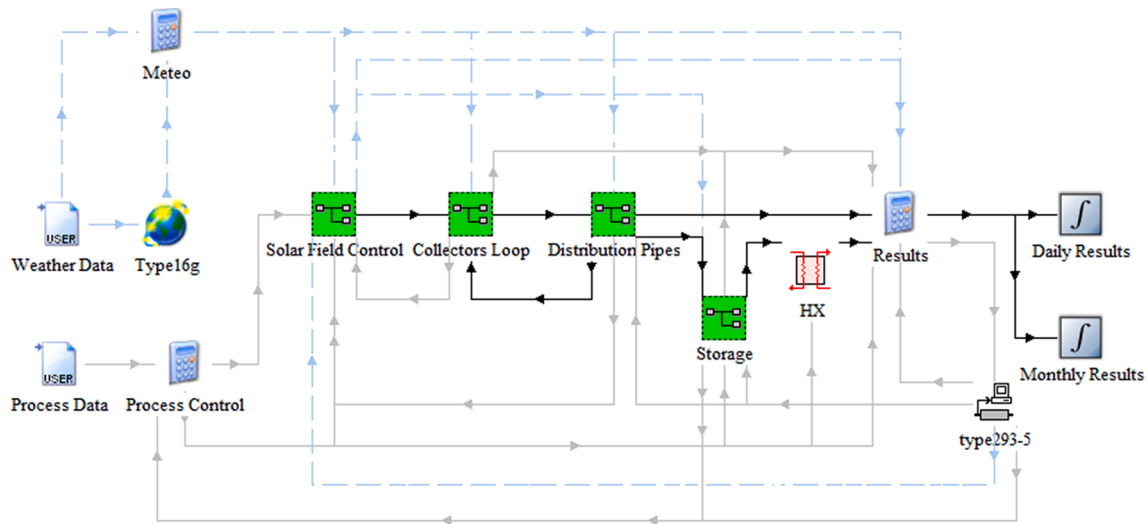

Fig. 3. Screenshot of the TRNSYS model for the whole system.

Table 3
Monthly DNI and average value of ambient temperature of Graz [37] and PSA [38].

Month	Graz, Austria		PSA, Almería, Spain	
	DNI (kWh/m^2)	T_{amb} (°C)	DNI (kWh/m^2)	T_{amb} (°C)
Jan	62	−1.2	133	9.2
Feb	90	1.8	149	13.2
Mar	101	6.0	144	12.6
Apr	110	11.4	179	15.2
May	127	16.5	179	18.5
Jun	132	19.7	227	24.7
Jul	138	21.1	243	26.8
Aug	121	20.4	198	27.1
Sep	97	15.5	170	22.3
Oct	79	11.0	167	18.2
Nov	53	5.5	142	14.5
Dec	43	0.1	142	12.1
Annual	1154	10.7	2071	17.9

processes, energy balances regarding thermal inertia are applied to estimate the evolution of temperatures.

Two TRNSYS components developed in-house are included in the model of PTC loops: parabolic-trough collectors and insulated pipes connecting adjacent PTCs. In addition, the pipe model is applied to simulate feed and return piping in the TRNSYS macro-component for distribution pipes seen in Fig. 3.

In general terms, the thermal model of parabolic troughs is carried out by evaluating the useful power ($\dot{Q}_u$) by means of an energy balance between solar power absorbed by the system and thermal losses to the environment ($\dot{Q}_{loss}$):

$$\dot{Q}_u = \eta_{opt,0°}\eta_{clean}\eta_{sh}K(\theta)G_b cos(\theta)A_c - \dot{Q}_{loss} \tag{1}$$

Where G_b is the DNI, A_c the net collector aperture area, θ the incidence angle, $K(\theta)$ the incidence angle modifier, $\eta_{opt,0°}$ the peak optical efficiency, η_{clean} the cleanliness factor and η_{sh} the shadowing factor between adjacent collector rows. The values of incidence angle modifier $K(\theta)$ and thermal losses $\dot{Q}_{loss}$ for PolyTrough 1800 collector are obtained by means of polynomial expressions taken from the collector's characterization performed by Larcher et al. [29].

To reproduce a quasi-dynamic behaviour of the system in transient conditions, the model performs an energy balance taking into account the effect of thermal inertia due to the mass of fluid, m_{fluid}, and pipe, m_{pipe}, in a time step Δt. The useful energy absorbed by the fluid, $\dot{Q}_u\Delta t$, can be expressed as a sum of energy interchanged in each component. If the effect of kinetic energy due to fluid speed variation is neglected, the outlet temperature of the fluid at the collector's outlet, T_{out}, can be thus obtained knowing the rest of the elements in Eq. (2), where $\dot{m}$ is the mass flow rate, $\Delta \overline{T}_{pipe}$ and $\Delta \overline{T}_{fluid}$ the increase in average temperature of the pipe and the fluid, respectively, since the previous time step, $c_{p,pipe}$ and $c_{p,fluid}$ the specific heat capacity of pipe and fluid and T_{in} the temperature of the fluid at collector's inlet.

$$\dot{Q}_u \Delta t = m_{fluid} c_{p,fluid} \Delta \overline{T}_{fluid} + m_{pipe} c_{p,pipe} \Delta \overline{T}_{pipe} + \dot{m} c_{p,fluid} (T_{out} - T_{in}) \Delta t \quad (2)$$

If we assume that the average temperature increase in the current time step is the same for fluid ($\Delta \overline{T}_{fluid}$) and piping ($\Delta \overline{T}_{pipe}$), and is equal to the average increase of inlet and outlet temperatures, $\Delta \overline{T}_{fluid} = \Delta \overline{T}_{pipe} = (\Delta T_{in} + \Delta T_{out})/2$, an explicit function for the collector outlet temperature can be obtained from Eq. (2), thus enabling a simplified approach.

On the other hand, the component for connecting pipes is implemented with a model of thermal nodes composed of metal tube and thermal insulation (see [39]) whose properties are known. Then, an energy balance is applied to calculate thermal losses to the atmosphere due to convection and to the sky due to radiation. Additionally, a mechanism (described in [40]) is incorporated to this model to simulate in a simple way the effect of thermal inertia by means of exponential expressions.

A detailed description of the thermal and hydraulic model for both parabolic trough and insulated pipe TRNSYS components can be found in former works by the authors [40–42], along with their validation using experimental results. According to this validation, 2–5% uncertainty in terms of thermal energy can be expected for the simulation of solar fields with this model.

Table 4 summarizes the main parameters applied in the SF model, in addition to the manufacturer's data values in Table 1, including PTCs, connecting pipes between collectors and distribution pipes.

3.3. Storage system model

The main functionality of the storage system is performed by a new TRNSYS component that models a simplified Latent Heat Storage (LHS) tank filled with a Phase Change Material (PCM). The LHS interchanges thermal energy with a flow of water, which may yield energy to the PCM in a charge process, or retrieve energy from the PCM in a discharge process.

The same properties are considered for the whole PCM mass and heat losses are neglected. The maximum storage capacity is equal to the phase change enthalpy of the total PCM mass. Hence, the storage level is calculated as the ratio of thermal energy stored in the PCM to the maximum storage capacity. The relative level of storage in the tank will be 0 for a tank with no latent heat stored, which represents an empty storage, or 1 for a full storage level.

The exchanged thermal power, $\dot{Q}$, is calculated by means of a simplified heat balance considering the heat transfer coefficient U, the heat transfer area A and the temperature difference between the HTF and the PCM ($T_{HTF} - T_{PCM}$), as described by equation (3):

$$\dot{Q} = U \cdot A \cdot (T_{HTF} - T_{PCM}) \quad (3)$$

Typically, a LHS device presents a heat transfer coefficient that varies with storage load. This effect is particularly relevant when the PCM has a low thermal conductivity, like in this case. For this study, an approach based on a linear evolution of the heat transfer coefficient is applied, obtaining U as function of the current storage level x:

$$U = C_1 \cdot x + C_o \quad (4)$$

C_0 and C_1 depend on the properties of the storage material, mainly the thermal diffusivity, the layout, geometry and features of the storage device and heat transfer surface. Also, they vary for charging and discharging cycle. Both parameters can be derived from either detailed models or experimental results.

In this case, the coefficients for Eq. (4) in charge or discharge processes have been inferred from the analysis of an experimental LHS device, the DISTOR facility [43]. In the DISTOR prototype, a eutectic mixture of KNO_2 and $NaNO_2$ was used as PCM, including graphite fins every cm that improved the bulk effective thermal diffusivity by an order of magnitude. Since the details of the design of the LHS device are not defined in the present study, a similar enhancement on the thermal diffusivity of PG is assumed (for example, by encapsulating it with an appropriate size, with a finned system, etc.). Considering that the heat transfer area of the DISTOR experimental setup is 10 m^2, the resulting values of heat transfer coefficient U for each process are depicted in Fig. 4.

The operating range for latent heat storage corresponds to the time period with constant temperature of the PCM. In Fig. 4, the phase transition starts for both charge and discharge processes at 0:04 (marked with dashed grey line). The specific point in which the end of phase transition occurs (i.e., the PCM temperature is no longer constant) for either charge or discharge processes is marked on each curve with dashed vertical lines (blue for charge, orange for discharge). In addition, linear approximations for each curve are also displayed in the same graph for the latent heat range, thus justifying the approach adopted in Eq. (4). A maximum difference of 30.9 W/m^2·K in charge or 28.3 W/m^2·K in discharge is observed between the experimental data and the linear approximation, whereas the corresponding root mean squared error (RMSE) is 15.3 W/m^2·K for charge or 13.7 W/m^2·K for discharge.

The main parameters considered in the storage system model are gathered in Table 5.

The total mass of PCM and the stored energy specified in Table 5 have been chosen to provide almost 3 h of operation at nominal thermal power. The heat transfer area has been obtained by extrapolating the value of the DISTOR facility [43] for the thermal capacity used in this study.

3.4. Operation and control strategies

The inclusion of thermal energy storage allows the proposed system

Table 4
Main parameters considered in the simulation model of the collectors' loop and distribution pipes in the solar field.

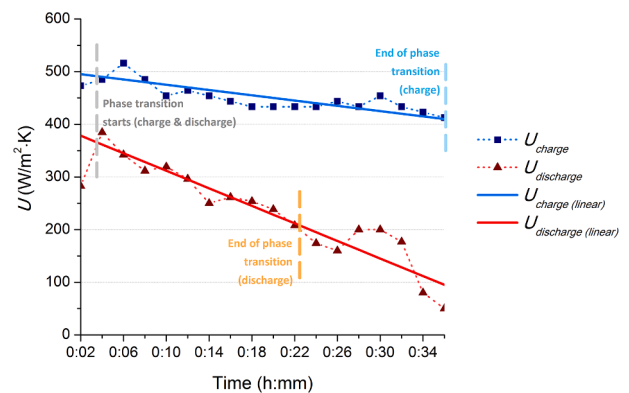| Parameter	Value
Peak optical efficiency of solar collectors (%)	69.5
Cleanliness factor of collectors' mirrors (%)	97
Total length of absorber tubes per loop (m)	40
Total length of connecting pipes per loop (m)	16
Outer diameter of connecting pipes (mm)	48
Inner diameter of connecting pipes (mm)	41
Insulation thickness of connecting pipes (mm)	26
N° elbows in connecting pipes	36
Length of return pipe (m)	100
Length of feed pipe (m)	150
Outer diameter of return/feed pipe (mm)	102
Inner diameter of return/feed pipe (mm)	90
Insulation thickness of return/feed pipe (mm)	100
N° elbows in return pipe	20
N° elbows in feed pipe	24

Fig. 4. Heat transfer coefficients for charge and discharge processes, together with linear approximations of each curve, for the experimental LHS device considered [43]

Table 5
Main parameters considered in the simulation model of the LHS system.

Parameter	Value
Thermal capacity (kWh)	800
Phase change temperature (°C)	85*
Phase change enthalpy (kJ/kg)	192 [31]
PCM mass (kg)	15,000
Heat transfer area (m^2)	100
C_0 charge (W/m^2·K)	500
C_1 charge (W/m^2·K)	−100
C_0 discharge (W/m^2·K)	200
C_1 discharge (W/m^2·K)	200

(*) According to our preliminary assessment results.

to fulfil the process demand either when fluid conditions in the SF are sufficient, in terms of temperature and mass flow rate, or when the TES system is charged. However, the different temperature levels required by the specific process and the use of a LHS system impose additional constraints to the coupling of SF + TES system with the IP that should be properly addressed.

To that end, operation modes are defined to cover the entire range of conditions that may occur both in the SF and the storage system according to relevant system variables, along with the process demand profile. Solar radiation, temperatures in the SF and the IP and storage load are the main inputs for triggering the operation modes considered in the simulation model, namely:

- **Solar field start-up**: during the first hours of the day or after deep cloudy transients, the temperature of the HTF is usually low and hence the SF is not able to provide the required conditions to feed the IP or to charge the TES system. Under such circumstances, SF operation is addressed to achieve nominal conditions as soon as possible, avoiding at the same time a non-uniform heating of the circuit that may suppose a risk of damage on specific points of the installation. To this end, a constant mass flow rate ($\dot{m}_{startup}$) is established that is high enough to ensure an approximately homogeneous heating rate in the SF. In this case the bypass line is used to enable the stand-alone operation of the SF by avoiding circulation through the HX or the TES system (see Fig. 5).

- **Regular operation**: when nominal conditions are achieved and the SF (including the support of the storage system) is able to supply the heat demanded by the IP, regular operation can be considered. Then, the HTF conditions should be carefully controlled according to solar irradiance and SF variables. The mass flow rate required to achieve the desired set-point temperature at the SF outlet ($T_{out,SF,ref}$) is calculated with Eq. (5), based on Eq. (1) and a simplified energy balance for steady-state conditions.

$$\dot{m}_{SF} = \frac{\eta_{opt,0°}\eta_{clean}\eta_{sh}K(\theta)G_b cos(\theta)A_c - \dot{Q}_{loss}}{c_{p,fluid}\left(T_{out,SF,ref} - T_{in,SF}\right)} \quad (5)$$
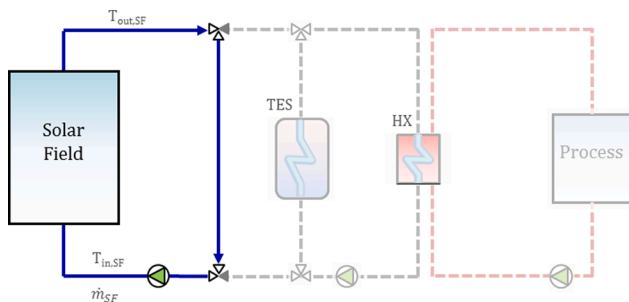
Regular operation can be subdivided into additional operation

modes depending on SF conditions, TES state and process demand:

- o **TES charge with no process demand**: when the outlet temperature of the heat transfer fluid ($T_{out,SF}$) is sufficient to charge the TES system and there is no heat demand from the IP ($\dot{m}_{IP,HTF} = 0$), the total amount of fluid from the SF can be driven to the storage system until it is fully charged. Since the inlet temperature to the SF is defined by the outlet temperature of the TES system, the set-point temperature at the SF outlet ($T_{out,SF,ref}$) is established by adding to the phase change temperature of the PCM (T_{PCM}) the nominal temperature difference expected between HTF and PCM in a charge process ($\Delta T_{TES,charge}$) and the desired temperature increase (ΔT_{SF}) in the SF: $T_{out,SF,ref} = T_{PCM} + \Delta T_{TES,charge} + \Delta T_{SF}$. A simplified diagram is displayed in Fig. 6 for this operation mode.

- o **TES charge with process demand**: when the temperature conditions of the HTF are sufficient to feed both the IP and the storage system ($T_{out,SF,ref} > T_{PCM} + \Delta T_{TES,charge}$) and the mass flow rate from the SF is higher than the required demand of the IP ($\dot{m}_{SF} > \dot{m}_{IP,HTF}$), the excess fluid can be driven to the storage system until it is fully charged (see Fig. 7). In this case the set-point temperature ($T_{out,SF,ref}$) is established by adding to the inlet temperature required by the process fluid ($T_{in,IP}$) the nominal temperature difference ($\Delta T_{HX,hot}$) expected at the hot side of the HX: $T_{out,SF,ref} = T_{in,IP} + \Delta T_{HX,hot}$.

When the storage system is completely full (TES_load = 1) in any TES charge mode, either with or without process demand, some of the solar collectors must be defocused to avoid the HTF overheating. Also, the mass flow rate in the SF should be reduced to the value required by the IP (zero if there is no demand).

- o **TES discharge with SF support**: when the storage system is charged (TES_load > 0) and the HTF is circulating through the SF but its mass flow rate is not enough to feed the IP ($0 < \dot{m}_{SF} < \dot{m}_{IP,HTF}$), the TES can be discharged at a specified mass flow rate to complement the SF support, being mixed with the SF fluid, and thus meet the required demand (see Fig. 8).

In order to attain the HTF temperature required by the IP at the HX inlet ($T_{in,HX,HTF}$), the set-point temperature at the SF outlet ($T_{out,SF,ref}$) must be adjusted to regulate the resulting temperature of the mixed flow with eq. (6):

$$T_{out,SF,ref} = T_{out,TES} - (T_{out,TES} - T_{in,HX,HTF})\frac{\dot{m}_{IP,HTF}}{\dot{m}_{SF}} \quad (6)$$

- o **TES discharge without SF support**: when the storage system is charged (TES_load > 0) but no useful fluid is flowing through the SF ($\dot{m}_{SF} = 0$), the TES can be discharged to feed the IP, provided that there is heat demand ($\dot{m}_{IP,HTF} > 0$) and the required temperature is within a suitable range for the TES system (Fig. 9).
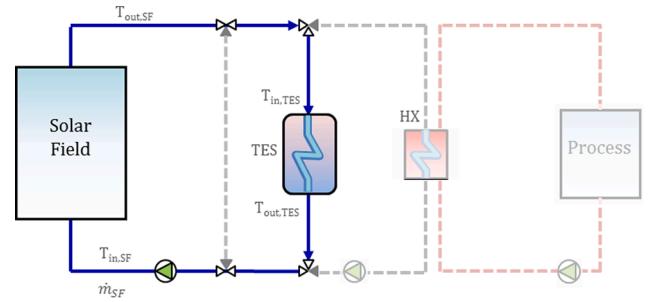

Fig. 5. Simplified diagram of the system operating in start-up mode.

Fig. 6. Simplified diagram of the system operating in TES charge mode with no process demand.
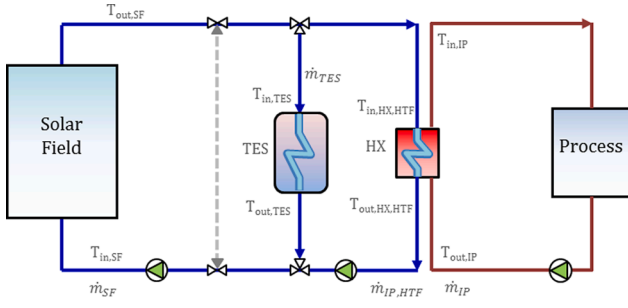
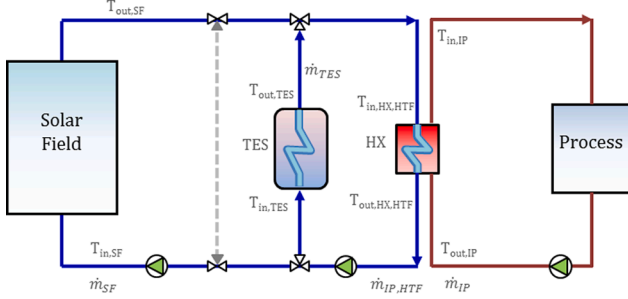**Fig. 7.** Simplified diagram of the system operating in TES charge mode with process demand.

Fig. 8. Simplified diagram of the system operating in TES discharge mode with SF support.
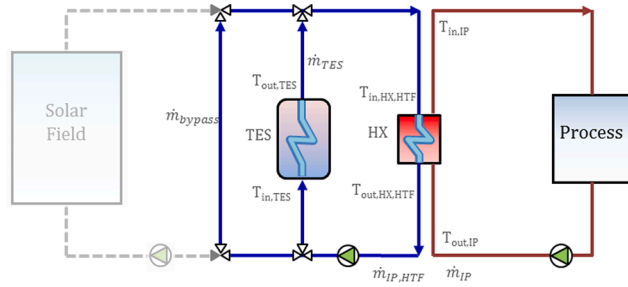

Fig. 9. Simplified diagram of the system operating in TES discharge mode without SF support.

The bypass line in Fig. 9 is used to cool down the fluid obtained from the TES system, thus adjusting the temperature of the mixed flow at the HX inlet ($T_{in,HX,HTF}$) to the value required by the IP. The corresponding mass flow rates through the bypass line and the TES system are calculated with the following expressions:

$$\dot{m}_{bypass} = \frac{T_{out,TES} - T_{in,HX,HTF}}{T_{out,TES} - T_{out,HX,HTF}} \dot{m}_{IP,HTF} \tag{7}$$

$$\dot{m}_{TES} = \dot{m}_{IP,HTF} - \dot{m}_{bypass} = \frac{T_{in,HX,HTF} - T_{out,HX,HTF}}{T_{out,TES} - T_{out,HX,HTF}} \dot{m}_{IP,HTF} \tag{8}$$

In both TES discharge modes (with or without SF support), the outlet temperature of the HTF obtained from the TES system ($T_{out,TES}$) is fixed by the phase change temperature of the PCM (T_{PCM}) and the temperature difference between PCM and HTF in discharge processes ($\Delta T_{TES,discharge}$), that is: $T_{out,TES} = T_{PCM} - \Delta T_{TES,discharge}$. Hence, the HTF temperature required by the IP at the HX inlet ($T_{in,HX,HTF} = T_{in,IP} + \Delta T_{HX,hot}$) must not be above the outlet temperature of the HTF from the TES system ($T_{in,HX,HTF} \leq T_{out,TES}$).

o **Solar-only mode**: when the storage system is fully charged (TES_load = 1) or the mass flow rate in the SF is lower than the required

demand of the IP ($\dot{m}_{SF} < \dot{m}_{IP,HTF}$) but it cannot be supported by the TES system, and temperature conditions of the SF fluid are sufficient to feed the IP, the system is operated in solar-only mode (see Fig. 10). In case the mass flow rate from the SF is higher than the required demand of the IP ($\dot{m}_{SF} > \dot{m}_{IP,HTF}$), solar collectors should be partially defocused to avoid the HTF overheating.

- **Circulation for antifreeze protection**: when fluid temperature is below a safety limit (10 °C), the HTF should be circulated with a minimum mass flow rate ($\dot{m}_{antifreeze}$) to avoid cold points and enable homogenization of temperatures. Given the low freezing point of water compared to alternative fluids like thermal oil, no auxiliary heating systems are considered in the simulation model.
- **Shutdown**: this operation mode may apply either to the SF or to the TES circuit (or both of them), involving the stop of HTF circulation in the corresponding system. When solar conditions are not sufficient to operate the SF ($G_b < G_{b,min}$), or there is not heat demand from the IP and the TES system is full (TES_load = 1), fluid circulation is stopped and solar collectors are defocused, thus involving a **SF shutdown** mode. This mode should only be activated when either overheating or freezing risks for HTF are not expected. On the other hand, when the TES system is empty (TES_load = 0) and there is not heat supply from the SF able to charge it, or when the TES system is completely full (TES_load = 1) but there is not heat demand from the IP to discharge the stored energy, HTF circulation must be stopped through the TES system and therefore a **TES shutdown** occurs.

The above described operation modes are summarized in Table 6, also including the conditions to activate each mode and the main calculations involved for set-point temperatures and mass flow rates.

The specific parameters applied for the management of operation modes and strategies in the simulation model are collected in Table 7.

4. Results and discussion

4.1. Thermal behaviour of pentaglycerine (PG)

In order to check the validity of pentaglycerine as SS-PCM in the temperature range of the IP application, preliminary thermal tests were carried out. The testing device consists in a small oven (4 l volume) with forced ventilation, which allows performing both heating and cooling ramps under controlled rate. For the thermal tests, glass tubes were filled with about 5 g of solid pentaglycerine. Two kinds of samples were tested at the same time: one sample with pentaglycerine as received, i.e., in grain form and another sample with pentaglycerine previously grinded to a fine powder in an agate mortar.

T-type thermocouples were inserted inside the samples for recording the temperature evolution with time. Oven temperature was monitored as well with another T-type thermocouple located between the tubes containing the samples. Fig. 11 displays the sample arrangement inside the oven.

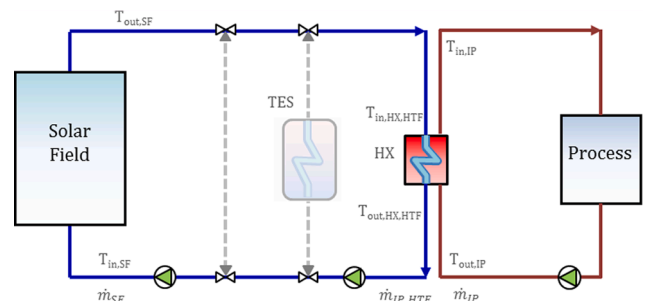Thermal tests consisted in heating/cooling runs performed from

Fig. 10. Simplified diagram of the system operating in solar-only mode.

Table 6

Operation modes, activating conditions and main calculations of set-point values in the simulation model.

Operation mode	Activating conditions	SF outlet temp. set-point ($T_{out, SF, ref}$)	Mass flow rates
SF start-up	$G_b \geq G_{b,min}$ & $T_{out,SF} < T_{PCM} + \Delta T_{TES,charge}$ & $T_{out,SF} < T_{in,IP} + \Delta T_{HX,hot}$	–	$\dot{m}_{SF} = \dot{m}_{startup}$
TES charge without IP demand	$G_b \geq G_{b,min}$ & $\dot{m}_{IP,HTF} = 0$ & $T_{out,SF} \geq T_{PCM} + \Delta T_{TES,charge}$ & TES_load < 1	$T_{PCM} + \Delta T_{TES,charge} + \Delta T_{SF}$	Eq. (5)
TES charge with IP demand	$G_b \geq G_{b,min}$ & $\dot{m}_{SF} > \dot{m}_{IP,HTF} > 0$ & $T_{out,SF,ref} > T_{PCM} + \Delta T_{TES,charge}$ & TES_load < 1	$T_{in,IP} + \Delta T_{HX,hot}$	Eq. (5) & $\dot{m}_{TES} = \dot{m}_{SF} - \dot{m}_{IP,HTF}$
TES discharge with SF support	$G_b \geq G_{b,min}$ & TES_load > 0 & $0 < \dot{m}_{SF} < \dot{m}_{IP,HTF}$ & $T_{out,TES} \geq T_{in,IP} + \Delta T_{HX,hot}$	Eq. (6)	Eq. (5) & $\dot{m}_{TES} = \dot{m}_{IP,HTF} - \dot{m}_{SF}$
TES discharge without SF support	TES_load > 0 & $\dot{m}_{SF} = 0$ & $\dot{m}_{IP,HTF} > 0$ & $T_{out,TES} \geq T_{in,IP} + \Delta T_{HX,hot}$	–	Eqs. (7) & (8)
Solar-only	$G_b \geq G_{b,min}$ & (TES_load = 1 OR ($\dot{m}_{SF} < \dot{m}_{IP,HTF}$ & $T_{out,TES} < T_{in,IP} + \Delta T_{HX,hot}$)) & $T_{out,SF} \geq T_{in,IP} + \Delta T_{HX,hot}$	$T_{in,IP} + \Delta T_{HX,hot}$	Eq. (5) & $\dot{m}_{SF} \leq \dot{m}_{IP,HTF}$
Antifreeze protection	$G_b < G_{b,min}$ & $T_{out,SF} < T_{antifreeze}$	–	$\dot{m}_{SF} = \dot{m}_{antifreeze}$
SF shutdown	($G_b < G_{b,min}$ OR (TES_load = 1 & $\dot{m}_{IP} = 0$)) & $T_{out,SF} \geq T_{antifreeze}$	–	$\dot{m}_{SF} = 0$
TES shutdown	(TES_load = 0 & $\dot{m}_{SF} = 0$) OR (TES_load = 1 & $\dot{m}_{IP} = 0$)	–	$\dot{m}_{TES} = 0$

Table 7

Main parameters considered in the simulation model for handling operation modes and strategies.

| Parameter	Value
Nominal temperature increase in the SF, ΔT_{SF} (°C)	7
Nominal temperature difference in hot side of HX, $\Delta T_{HX,hot}$ (°C)	6
Nominal temperature difference in cold side of HX, $\Delta T_{HX,cold}$ (°C)	6
Nominal temperature difference between HTF and PCM during charge, $\Delta T_{TES,charge}$ (°C)	4
Nominal temperature difference between PCM and HTF during discharge, $\Delta T_{TES,discharge}$ (°C)	4
Phase change temperature of PCM, T_{PCM} (°C)	85
Temperature for antifreeze protection, $T_{antifreeze}$ (°C)	10
Minimum DNI for SF operation, $G_{b,min}$ (W/m^2)	20
SF mass flow rate during start-up, $\dot{m}_{startup}$ (kg/s)	6.4
SF mass flow rate for antifreeze protection, $\dot{m}_{antifreeze}$ (kg/s)	2.4
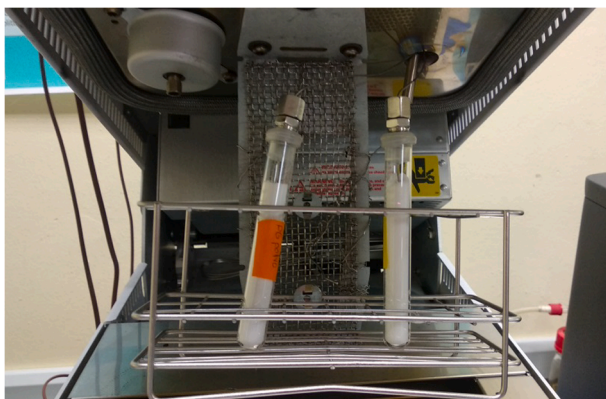
Fig. 11. Pentaglycerine samples arrangement inside the oven where thermal tests were performed.

50 °C to 100 °C at various rates (2, 3, 5, 7, 10 and 20 °C/min) with stand-by periods of 20 min at constant temperature between each ramp. In Fig. 12 temperature evolution curves of the oven and the two PG samples (as-received grain and grinded powder) are displayed for the tests at 2, 3 and 7 °C/min.

During heating, the temperatures of both PG samples follow the temperature increase of the oven until SS-transition temperature is reached. From this moment a plateau is clearly observed for the grinded powder sample due to the phase transition. In contrast, for the sample in grain form only a change in temperature slope is observed. During cooling, a similar behaviour is observed. While the sample of grinded powder presents a clear plateau at around SS transition temperature, the sample of as-received grain only shows a small shoulder. Comparing with the sample with the as-received PG, the grinded powder sample contains much smaller solid particles and this leads to an improvement of the heat transfer, not only between adjacent particles but also between the particles and the thermocouple that records the sample temperature. This is why the sample of grinded powder presents a temperature–time curve similar to one displayed by the conventional PCM with solid–liquid transitions in which the sample is in full contact with the thermocouple [44].

In Fig. 12 we also observe that SS-transition of pentaglycerine takes place at constant temperature around 85 °C for all the heating/cooling rates tested and no relevant supercooling occurs during the cooling process. Hence, PG is expected to work properly regardless of the thermal gradient between the HTF and the storage system, so that it can be an appropriate latent storage material for the application under study.

4.2. Full day simulation

In order to observe the system behaviour along an entire daytime, a typical spring sunny day has been selected to represent circuit variables obtained from the simulation. In this way, Fig. 13 shows the daily evolution of SF and process temperatures, thermal power and TES load, including DNI, for the 5th of April in Graz.

The results seen in Fig. 13 are helpful to understand the behaviour of the simulation model regarding the various operation strategies defined in Section 3.4. Time regions are delimited with dashed vertical grey lines to better observe the different operation modes the system can undergo depending on circuit conditions.

Firstly, corresponding to night time with no solar radiation, region (0) represents shutdown conditions both for SF and TES system. In time region (I), when the available solar radiation reaches a threshold value, fluid circulation is started to heat up the working fluid (without charging the TES system) and thus the SF is in startup mode. When the fluid attains the temperature required for a TES charge process, the useful heat can be then delivered to the storage system. Since there is no heat demand from the IP, during time region (II) the system is in TES charge mode without process demand. This mode finishes when the storage
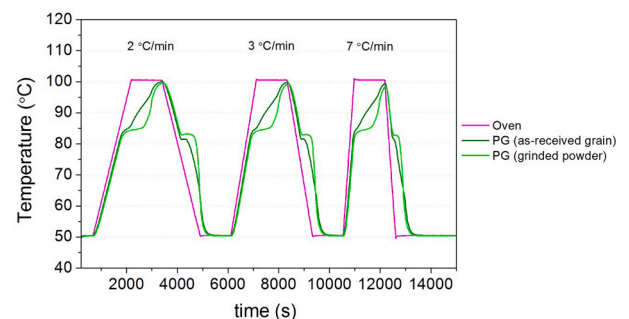

Fig. 12. Temperature evolution of pentaglycerine (PG) samples in grain or grinded powder form during heating/cooling tests performed at 2, 3 and 7 °C/min.
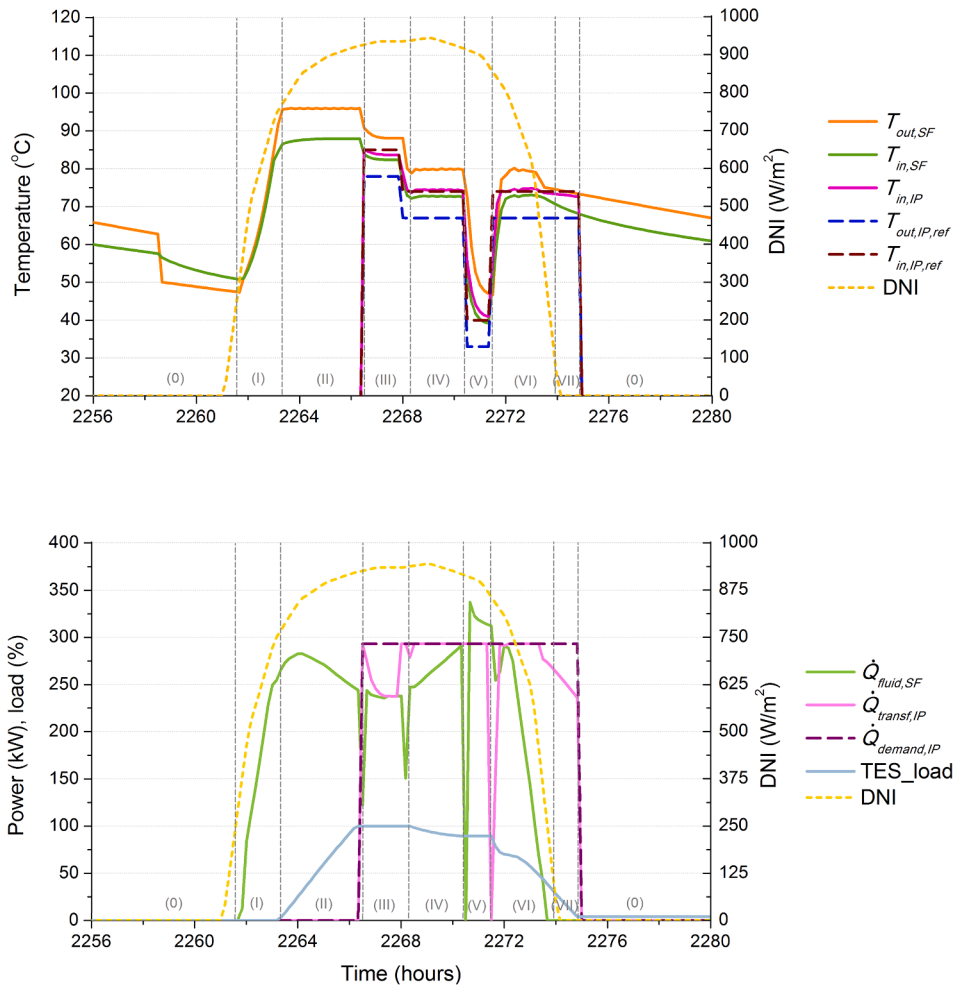
Fig. 13. Daily evolution of SF and process temperatures, thermal power and TES load, including DNI, for a sunny day of spring (5th of April) in Graz.

system is fully charged, entering region (III).

Coincidentally, the industrial heat demand starts with region (III), at the same time as the storage load reaches its full level. In this case, the SF is not capable of providing the whole amount of thermal power demanded. Nevertheless, the temperature level required by the process does not allow the storage system to complete the support of the SF; hence the system is operated in solar-only mode to feed the pasteurization process. In region (IV), however, the required temperature level is lower and both flows from SF and TES system are mixed to supply the heat demanded by IP. The system operates then in TES discharge with SF support.

In region (V) the temperature level required by the process significantly decreases and the SF can supply by itself the total amount of heat demanded, with the system operating in solar-only mode. The temperature required by the pasteurization process increases again during region (VI), making the system to operate in TES discharge mode with SF support until solar radiation is below a threshold value. At this moment, in region (VII) the IP is fed exclusively by the TES system, corresponding to a TES discharge mode without SF support. Finally, when there is neither solar radiation nor available heat stored, the system goes again into shutdown mode (region (0)).

4.3. Overall yield results

Simulations have been carried out throughout one year using the model described in Section 3 for the two locations considered: Graz and PSA. Since meteorological data and IP input data do not have the same time step, the missing values have to be interpolated. Hence, for Graz

location, simulation step is 10 min and weather data are interpolated, whereas for PSA, simulation step is 5 min and in this case IP data are interpolated.

In order to assess the impact of the proposed LHS system, the overall results of thermal energy delivered to the IP for a certain period (daily, monthly) by the above-described system with 3 h of TES are compared to an alternative system using the same SF but no thermal storage at all. Besides, the total demand of the IP in terms of thermal energy is taken as reference since the remaining energy that cannot be provided by the SF and/or TES needs to be supplied by an auxiliary boiler. In this way, the corresponding results of thermal energy yield are represented as percentage of the overall demand of the IP.
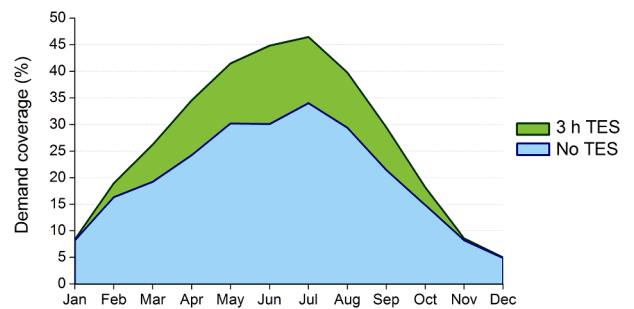

Fig. 14. Monthly thermal energy delivered to the process (with 3 h TES or with no TES), as percentage of the total demand, using meteorological data of Graz, Austria.

Firstly, Fig. 14 displays the monthly results of thermal energy delivered to the process (with 3 h TES, in green, or with no TES, in blue), as percentage of the total demand, using meteorological data of Graz.

As shown in Fig. 14, the simulation with 3 h TES is capable of covering up to 45–46% of the process demand in June-July, whereas 30–34% is reached for the same months in the simulation without storage. To summarize, results are 10–15 percent points higher with 3 h TES than without storage in summer months (from April to August). However, the coverage is almost equal for both options in winter months, leading to differences lower than 4 percent points from October to February.

On the other hand, the proportion of energy dumping is calculated as the ratio of annual thermal energy not used due to solar collectors defocusing (because the storage is already full or not existent) to the total energy delivered to the process. As a result, 2% of annual energy with 3 h TES or 35% without storage is dumped, thus reflecting a better use of the available solar resource thanks to the proposed storage system.

Since monthly values gather cumulative results, the system behaviour for individual days is not considered in the figures above. Nonetheless, it is also interesting to analyse the daily coverage of the demand to better observe at what extent the SF and TES can feed by themselves the IP. To that purpose, daily results of thermal energy delivered to the process for a whole year (with 3 h TES, in green, or with no TES, in blue), as percentage of the total demand, using meteorological data of Graz are represented in Fig. 15.

As seen in Fig. 15, in 24 days of the year the system with 3 h TES would be able to cover most of the daily process demand (>90%), whereas the value obtained with no storage is significantly lower (60–80% of the demand). Such coverage only occurs in certain days of summer with good weather conditions. On the other hand, most days of winter the system with TES can only deliver an amount of heat similar to the one obtained without storage, thus making the TES system useless for these days.

To compare with a location that presents higher values of annual DNI, Fig. 16 shows the monthly results of thermal energy delivered to the process (with 3 h TES, in green, or with no TES, in blue), as percentage of the total demand, using meteorological data of the PSA.

In this case, every month of the year the results are higher for the system with thermal storage. Nevertheless, the results are more advantageous in summer (15–18 percent points from April to August) than in winter months (6–10 percent points from September to March).

The proportion of annual thermal energy dumped, with respect to the total energy delivered to the process, is 9% with 3 h TES or 29% without storage. Therefore, the difference between both options in terms of energy dumping factor is lower for the PSA than in the case of Graz. Nevertheless, this effect is related to the overall amount of energy involved for locations with higher annual DNI, leading to bigger differences in absolute terms, but smaller in relative terms.

Finally, the daily results of thermal energy delivered to the process for a whole year (with 3 h TES, in green, or with no TES, in blue), as percentage of the total demand, using meteorological data of the PSA are depicted in Fig. 17.
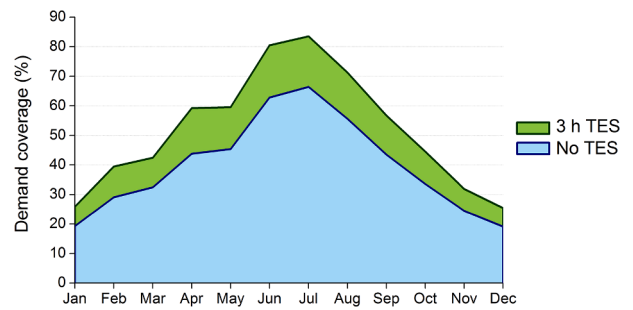

Fig. 16. Monthly thermal energy delivered to the process (with 3 h TES or with no TES), as percentage of the total demand, using meteorological data of PSA, Spain.

As inferred from Fig. 17, in 62 days of the year the system with 3 h TES is able to cover more than 90% of the daily process demand, whereas the system without storage never reaches this proportion. Moreover, almost every day the percentage of the demand covered with 3 h TES is higher than the one covered without storage, even in winter. The better annual behaviour observed for the PSA, compared to Fig. 15 for Graz, suggests that the advantages of a TES system such as the one proposed in this work are more evident for locations with high annual DNI values.

The annual solar fractions obtained for the PSA (52% with 3 h TES, 40% with no TES) are within the expected ranges reported for similar applications and latitudes (17–67% with TES in hot water tanks, according to [6,12,15–17]). Nevertheless, the final energy output will strongly depend on the SHIP system features, collection area, climate data, etc. Therefore, those figures should only be taken as a reference.

5. Conclusions

The use of latent heat storage systems can suppose several advantages in terms of availability and dispatchability of the heat production, as well as a better integration of solar fields to the daily demand of industrial processes.

This work presents a solution applied to a specific industrial process, a pasteurization procedure in a dairy factory, involving three different temperature levels, the highest of them up to 85 °C. A commercial parabolic-trough collector, NEP PolyTrough 1800, is selected to supply a part of the required heat demand by means of solar energy. The solar field layout is composed of 8 rows of solar collectors with 4 collectors per row. In addition, a LHS system using pentaglycerine as SS-PCM with about 3 h storage capacity is proposed to complement the solar field support, storing the remaining heat and releasing it when solar radiation is not available.

Experimental tests have been carried out by applying thermal cycles to different forms of pentaglycerine to confirm its suitability for the proposed application. Since a stable transition temperature around 85 °C and no relevant supercooling are observed, pentaglycerine seems to show a good behaviour regarding its use as a SS-PCM.
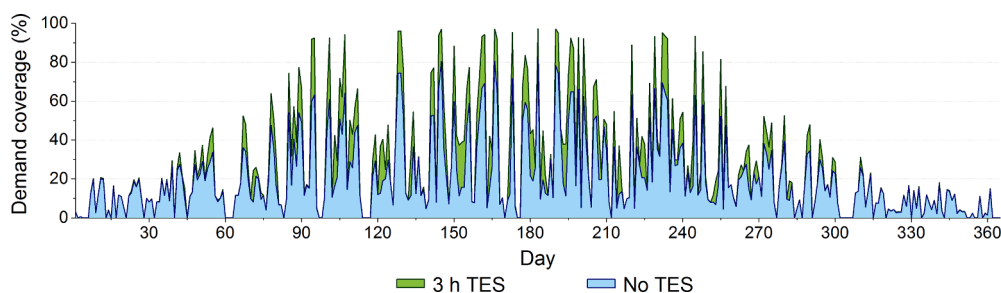

Fig. 15. Daily thermal energy delivered to the process (with 3 h TES or with no TES), as percentage of the total demand, using meteorological data of Graz, Austria.
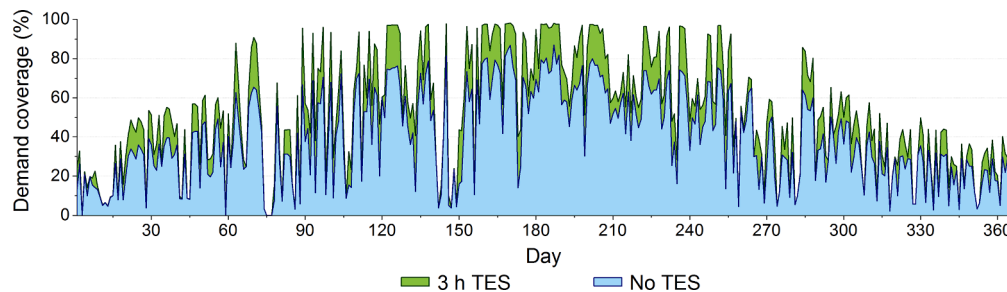
Fig. 17. Daily thermal energy delivered to the process (with 3 h TES or with no TES), as percentage of the total demand, using meteorological data of PSA, Spain.

A quasi-dynamic model is developed to simulate the transient behaviour of each component, yielding production results that enable the assessment of overall system performance. Also, a complete set of operation modes, able to represent all the operating conditions that may occur in such installation, is defined and implemented in the simulation model. This enables the control system of the SHIP facility to deal with the variable temperature values required by the industrial process by means of the regulation of the mass flow rate through each subsystem.

Two different locations are considered for the simulations: Graz (Austria) and Plataforma Solar de Almería (Spain). The annual thermal energy production using the proposed storage system is compared to that with the same solar field but without storage. As a result, the solar fraction, i.e. the percentage of the annual heat demand of the industrial process that can be covered with 3 h of LHS is 27% for Graz or 52% for the PSA, whereas the expected coverage without storage is 20% for Graz or 40% for the PSA. In addition to the resulting increase in the solar fraction, pentaglycerine may suppose further advantages when used as PCM in latent storage systems for SHIP applications: low cost of raw material, low expected degradation of PCM, low corrosion and stress in containers, possibilities of encapsulation or composites, etc. In this way, the solution proposed in this study may be an interesting research topic for SHIP concepts that include thermal energy storage. Moreover, the simulation model developed can be a useful tool to predict the expected behaviour and production of similar applications. For instance, the specific operation strategies defined in this work may also be applied to thermal storage systems with variable discharge curves, such as sensible heat storage with solid materials.

Declaration of Competing Interest

The authors declare that they have no known competing financial interests or personal relationships that could have appeared to influence the work reported in this paper.

Acknowledgements

References

[1] IEA Statistics data browser. http://iea.org/statistics [accessed on 2 December 2019].

[2] Solar Payback project. https://solar-payback.com [accessed on 3 December 2019].

[3] INSHIP – Integrating National Research Agendas on Solar Heat for Industrial Processes. http://www.inship.eu [accessed on 2 December 2019].

[4] L. Kumar, M. Hasanuzzaman, N.A. Rahim, Global advancement of solar thermal energy technologies for industrial process heat and its future prospects: A review, Energy Convers. Manage. 195 (2019) 885–908.

[5] A.K. Sharma, C. Sharma, S.C. Mullick, T.C. Kandpal, Solar industrial process heat: A review, Renew. Sustain. Energy Rev. 78 (2017) 124–137.

[6] A.K. Sharma, C. Sharma, S.C. Mullick, T.C. Kandpal, Potential of solar industrial process heating in dairy industry in India and consequent carbon mitigation, J. Cleaner Prod. 140 (2017) 714–724.

[7] IEA Task 49 Solar Heat for Industrial Processes – SHIP Database – Database of Solar Heat Applications in Industrial Processes. http://ship-plants.info [accessed on 2 December 2019].

[8] SOLRICO. http://www.solrico.com [accessed on 15 May 2020].

[9] W. Weiss, M. Spörk-Dür, Solar Heat Worldwide, 2019 Edition, IEA Solar Heating & Cooling Programme. https://www.iea-shc.org/Data/Sites/1/publications/Solar-Heat-Worldwide-2019.pdf, May 2019 [accessed on 15 May 2020].

[10] B. Koçak, A.I. Fernandez, H. Paksoy, Review on sensible thermal energy storage for industrial solar applications and sustainability aspects, Sol. Energy 209 (2020) 135–169.

[11] A. Crespo, C. Barreneche, M. Ibarra, W. Platzer, Latent thermal energy storage for solar process heat applications at medium-high temperatures – A review, Sol. Energy 192 (2019) 3–34.

[12] A. Baniassadi, M. Momen, M. Amidpour, O. Pourali, Modeling and design of solar heat integration in process industries with heat storage, J. Cleaner Prod. 170 (2018) 522–534.

[13] C. Maillot, J. Castaing-Lasvignottes, O. Marc, Modeling and dynamic simulation of solar heat integration into a manufacturing process in Réunion Island, Procedia Manuf. 35 (2019) 118–123.

[14] S. Lugo, O. García-Valladares, R. Best, J. Hernández, F. Hernández, Numerical simulation and experimental validation of an evacuated solar collector heating system with gas boiler backup for industrial process heating in warm climates, Renew. Energy 139 (2019) 1120–1132.

[15] M. Bolognese, D. Viesi, R. Bartali, L. Crema, Modeling study for low-carbon industrial processes integrating solar thermal technologies. A case study in the Italian Alps: The Felicetti Pasta Factory, Sol. Energy 208 (2020) 548–558.

[16] R. Silva, M. Pérez, A. Fernández-García, Modeling and co-simulation of a parabolic trough solar plant for industrial process heat, Appl. Energy 106 (2013) 287–300.

[17] A. Allouhi, Y. Agrouaz, M. Benzakour-Amine, S. Rehman, M.S. Buker, T. Kousksou, A. Jamil, A. Benbassou, Design optimization of a multi-temperature solar thermal heating system for an industrial process, Appl. Energy 206 (2017) 382–392.

[18] A. Fallahi, G. Guldentops, M. Tao, S. Granados-Focil, S. Van Dessel, Review on solid-solid phase change materials for thermal energy storage: Molecular structure and thermal properties, Appl. Therm. Eng. 127 (2017) 1427–1441.

[19] H. Singh, A. Talekar, W.-M. Chien, R. Shi, D. Chandra, A. Mishra, M. Tirumala, D. J. Nelson, Continuous solid-state phase transitions in energy storage materials with orientational disorder – Computational and experimental approach, Energy 91 (2015) 334–349.

[20] P. Hu, P.-P. Zhao, Y. Jin, Z.-S. Chen, Experimental study on solid–solid phase change properties of pentaerythritol (PE)/nano-AlN composite for thermal storage, Sol. Energy 102 (2014) 91–97.

[21] D. Mani, M.K. Saranprabhu, K.S. Rajan, Intensification of thermal energy storage using copper-pentaerythritol nanocomposites for renewable energy utilization, Renew. Energy 163 (2021) 625–634.

[22] K.P. Venkitaraj, B. Praveen, H. Singh, S. Suresh, Low melt alloy blended polyalcohol as solid-solid phase change material for energy storage: An experimental study, Appl. Therm. Eng. 175 (2020), 115362.

[23] S. Bazri, I.A. Badruddin, M.S. Naghavi, M. Bahiraei, A review of numerical studies on solar collectors integrated with latent heat storage systems employing fins or nanoparticles, Renew. Energy 118 (2018) 761–778.

[24] S. Bazri, I.A. Badruddin, M.S. Naghavi, O.K. Seng, S. Wongwises, An analytical and comparative study of the charging and discharging processes in a latent heat thermal storage tank for solar water heater system, Sol. Energy 185 (2019) 424–438.

[25] C. Pagkalos, G. Dogkas, M.K. Koukou, J. Konstantaras, K. Lymperis, M. G. Vrachopoulos, Evaluation of water and paraffin PCM as storage media for use in thermal energy storage applications: A numerical approach, Int. J. Thermofluids 1–2 (2020), 100006.

[26] B. Lamrani, A. Draoui, Modelling and simulation of a hybrid solar-electrical dryer of wood integrated with latent heat thermal energy storage system, Therm. Sci. Eng. Progress 18 (2020), 100545.

[27] J. Zhao, Y. Ji, Y. Yuan, Z. Zhang, J. Lu, Seven operation modes and simulation models of solar heating system with PCM storage tank, Energies 10 (12) (2017), 2128, https://doi.org/10.3390/en10122128.

[28] AEE-INTEC. AEE-Institute for Sustainable Technologies. Gleisdorf, Austria. https://www.aee-intec.at [accessed on 27 February 2020].

[29] M. Larcher, M. Rommel, A. Bohren, E. Frank, S. Minder, Characterization of a parabolic trough collector for process heat applications, Energy Procedia 57 (2014) 2804–2811.

[30] R. Bayón, New storage concepts for innovative SHIP concepts. INSHIP project report, February 2019.

[31] D.K. Benson, J.D. Webb, R.W. Burrows, J.D.O. McFadden, C. Christensen, Materials Research for Passive Solar Systems: Solid-State Phase-Change Materials. Solar Energy Research Institute. Golden, Colorado, US. Report No. SERI/TR-255-1828, U.S. Department of Energy, Contract No. EG-77-C-01-4042, March 1985.

[32] N. Zhang, Y. Song, Y. Du, Y. Yuan, G. Xiao, Y. Gui, A Novel Solid-Solid Phase Change Material: Pentaglycerine/Expanded Graphite Composite PCMs, Adv. Eng. Mater. 20 (10) (2018) 1800237.

[33] R. Christodoulaki, L. Valenzuela, M. Biencinto, L. González, INSHIP Dimensioning tool for the Balance of Plant of Solar Heat for Industrial Processes systems. Proceedings of the 25th SolarPACES Conference, 1-4 October 2019, Daegu, South Korea.

[34] S. Klein, et al., TRNSYS 17: A Transient System Simulation Program. Solar Energy Laboratory, University of Wisconsin, Madison, USA. http://sel.me.wisc.edu/trnsys, 2013 [accessed on 19 December 2016].

[35] H.B. Kim, C.C. Tadini, R.K. Singh, Heat transfer in a plate exchanger during pasteurization of orange juice, J. Food Eng. 42 (1999) 79–84.

[36] R. Kumar, A.K. Pataskar, Heat Enhancement of Plate Heat Exchanger Working Efficiency by Twist Tape Turbulator at different pitches in Dairy Milk Pasteurization System, Int. J. Eng. Trends Technol. 60 (2018) 45–50.

[37] Meteonorm. Meteotest AG. Bern, Switzerland. https://meteonorm.com/en/, 2019 [accessed 24 October 2019].

[38] PSA. Plataforma Solar de Almería, Spain. https://www.psa.es/en/, 2019 [accessed 3 March 2020].

[39] M. Biencinto, L. González, L. Valenzuela, A quasi-dynamic simulation model for direct steam generation in parabolic troughs using TRNSYS, Appl. Energy 161 (2016) 133–142.

[40] M. Biencinto, L. González, E. Zarza, L.E. Díez, J. Muñoz-Antón, Performance model and annual yield comparison of parabolic-trough solar thermal power plants with either nitrogen or synthetic oil as heat transfer fluid, Energy Convers. Manage. 87 (2014) 238–249.

[41] M. Biencinto, R. Bayón, E. Rojas, L. González, Simulation and assessment of operation strategies for solar thermal power plants with a thermocline storage tank, Sol. Energy 103 (2014) 456–472.

[42] M. Biencinto, L. González, L. Valenzuela, E. Zarza, A new concept of solar thermal power plants with large-aperture parabolic-trough collectors and sCO$_2$ as working fluid, Energy Convers. Manage. 199 (2019), 112030.

[43] R. Bayón, E. Rojas, L. Valenzuela, E. Zarza, J. León, Analysis of the experimental behaviour of a 100 kWth latent heat storage system for direct steam generation in solar thermal power plants, Appl. Therm. Eng. 30 (2010) 2643–2651.

[44] R. Bayón, M. Biencinto, E. Uranga, E. Rojas, Study of hybrid dry cooling systems for STE plants based on latent storage. Proceedings of International Sustainable Energy Conference ISEC 2018. 3-5 October 2018, Graz (Austria), p. 597.